HERG Channel (Dys)function Revealed by Dynamic Action Potential Clamp Technique

Géza Berecki,*† Jan G. Zegers,† Arie O. Verkerk,*† Zahurul A. Bhuiyan,‡ Berend de Jonge,* Marieke W. Veldkamp,* Ronald Wilders,† and Antoni C. G. van Ginneken*

*Experimental and Molecular Cardiology Group and the Departments of †Physiology and ‡Clinical Genetics, Academic Medical Center, University of Amsterdam, The Netherlands

ABSTRACT The human ether-a-go-go-related gene (HERG) encodes the rapid component of the cardiac delayed rectifier potassium current (I_{Kr}). Per-Arnt-Sim domain mutations of the HERG channel are linked to type 2 long-QT syndrome. We studied wild-type and/or type 2 long-QT syndrome-associated mutant (R56Q) HERG current (I_{HERG}) in HEK-293 cells, at both 23 and 36°C. Conventional voltage-clamp analysis revealed mutation-induced changes in channel kinetics. To assess functional implication(s) of the mutation, we introduce the dynamic action potential clamp technique. In this study, we effectively replace the native I_{Kr} of a ventricular cell (either a human model cell or an isolated rabbit myocyte) with I_{HERG} generated in a HEK-293 cell that is voltage-clamped by the free-running action potential of the ventricular cell. Action potential characteristics of the ventricular cells were effectively reproduced with wild-type I_{HERG}, whereas the R56Q mutation caused a frequency-dependent increase of the action potential duration in accordance with the clinical phenotype. The dynamic action potential clamp approach also revealed a frequency-dependent transient wild-type I_{HERG} component, which is absent with R56Q channels. This novel electrophysiological technique allows rapid and unambiguous determination of the effects of an ion channel mutation on the ventricular action potential and can serve as a new tool for investigating cardiac channelopathies.

INTRODUCTION

Discrete mutations in genes encoding ion channel proteins that disrupt channel function are at present the most commonly identified cause of heritable cardiac channelopathies (Marbán, 2002). Type 2 of the congenital long-QT (LQT2) syndrome is linked to mutations in the human ether-a-go-go-related gene (HERG), which encodes the pore-forming α-subunit of the rapid delayed rectifier potassium channel (Curran et al., 1995; Sanguinetti et al., 1995; Trudeau et al., 1995). Properties of current through HERG channels (I_{HERG}) are similar to those of the rapidly activating component of delayed rectifier K^+ current (I_{Kr}) that contributes to the final repolarization of the ventricular action potential (AP) (Sanguinetti and Jurkiewicz, 1990). Investigations of various (wild-type and mutant) HERG channels in heterologous expression systems such as *Xenopus laevis* oocytes or mammalian tissue cells in culture have provided remarkable results in understanding the congenital forms of the LQT2 syndrome. It is apparent that the mechanisms by which HERG mutations cause the clinically observed electrical disease are various. For some HERG mutants, the observed differences in HERG channel kinetics and/or I_{HERG} density are evident and translation into effects that these mutated channels would have on the ventricular AP are obvious. Conversely, in several cases, results of voltage-clamp experiments do not provide satisfactory explanation to how structural changes of the channel protein would affect cardiac AP repolarization and ultimately lead to the observed clinical phenotype in affected patients. In such cases, where the observed differences between the wild-type and mutant channels are less clear, one can in existing computer models of the human ventricular AP (Priebe and Beuckelmann, 1998) modify I_{Kr} according to what was found for the mutant and determine the resulting change(s) in AP characteristics. It is then, often implicitly, assumed that the mathematical description of the I_{Kr} fully covers the properties of this current. Besides, this approach is restrained by the lack of quantitative data on the complex kinetics of the I_{Kr} and I_{HERG} at physiological temperature. The mathematical description is therefore merely an approximation, despite recent advances in modeling (Clancy and Rudy, 2001), and results from simulations in which HERG channel properties have been changed should be interpreted circumspectly.

In this study, we introduce a novel electrophysiological technique to assess the functional implications of ion channel mutations. We hypothesize that rapid and unambiguous interpretation of the altered channel function is possible with an experimental setting in which mutant channels are allowed to follow a natural time course of membrane potential (V_m) change, upon being simultaneously allowed to contribute current to the AP as they would have when incorporated into a real ventricular cell. With our dynamic action potential clamp (dAPC) technique, the native I_{Kr} of a ventricular myocyte or cell model is effectively replaced with I_{HERG} recorded from a transfected HEK-293 cell that is voltage-clamped by the free-running AP of the ventricular cell. To this end, the native

Submitted June 8, 2004, and accepted for publication September 29, 2004.

Address reprint requests to G. Berecki, Dept. of Clinical and Experimental Cardiology, Academic Medical Center, University of Amsterdam, Rm. M01-217, Meibergdreef 9, 1105 AZ Amsterdam, PO Box 22700, 1100 DE Amsterdam, The Netherlands. Tel.: 31-20-566-7547; Fax: 31-20-691-9319; E-mail: g.berecki@amc.uva.nl.

0006-3495/05/01/566/13 $2.00

doi: 10.1529/biophysj.104.047290

I_{Kr} is pharmacologically blocked (or set to zero in case of a model cell) and I_{HERG} is applied to the ventricular cell as an external current input. When wild-type (WT) I_{HERG} is added to the net membrane current of this ventricular cell, the resulting AP should be considered as normal, whereas a mutant I_{HERG} should cause distortion of the AP.

We applied our dAPC technique to the R56Q (arginine to glutamine) mutation, a defect known to increase the rate of deactivation most profoundly (Chen et al., 1999). Previously, R56Q HERG channels had only been expressed in *Xenopus* oocytes, and characterized at room temperature (Chen et al., 1999). We studied WT and mutant channels in HEK-293 cells also by conventional whole-cell voltage-clamp technique, at both 23°C and 36°C. At physiological temperature, the mutant channels showed both faster deactivation, which would lengthen the AP, and faster activation, which by itself would shorten the AP. However, our dAPC experiments directly and unambiguously demonstrate that the net effect of the mutation is an increase in action potential duration (APD).

MATERIALS AND METHODS

Electrophysiological experiments

For details on plasmid construction, HEK-293 cell culture, and transfection procedures, see the expanded Materials and Methods, available as Supplementary Material online.

HEK-293 cells were either superfused with Tyrode's solution containing (mmol/L): 140 NaCl, 5.4 KCl, 1.8 $CaCl_2$, 1 $MgCl_2$, 5.5 glucose, 5 HEPES (pH 7.4 with NaOH), or with a modified Tyrode's solution with 4.5 instead of 5.4 mmol/L KCl (see below). Membrane currents were recorded with an Axopatch 200B amplifier (Axon Instruments, Union City, CA) in the whole-cell configuration of the patch-clamp technique at 23 ± 0.5°C and 36 ± 0.5°C. Voltage control, data acquisition, and analysis were accomplished using custom software. Patch pipettes (1.5–3 MΩ) were filled with solution containing (mmol/L): 125 K-gluconate, 20 KCl, 1 $MgCl_2$, 5 EGTA, 5 MgATP, 10 HEPES (pH 7.2 with KOH), resulting in a K^+ equilibrium potential (E_K) of −87.7 mV at 36°C. To obtain a better match between the E_K of the experimental solutions and the model cell's maximum diastolic potential of −90.7 mV, we also used 4.5 mmol/L KCl in the Tyrode solution (resulting in an E_K of −92.5 mV). All figures showing APs in the model-cell mode (see below) were obtained with this modified Tyrode solution. The pH of solutions was corrected for temperature; potentials were corrected for liquid junction potential. Membrane currents and potentials were low-pass filtered (cutoff frequency 2 kHz) and digitized at 5 kHz. The current-voltage (I-V) relationships, and I_{HERG} kinetics were determined by voltage-clamp protocols, as diagrammed in Figs. 2 and 3, and as described previously (Sanguinetti et al., 1995; Smith et al., 1996; Snyders and Chaudhary, 1996) and in the Supplementary Material. APs from freshly isolated rabbit left-ventricular myocytes were measured at 36°C with the solutions described above (5.4 mmol/L KCl in the Tyrode solution; EGTA was omitted in the pipette solution), as described previously (Verkerk et al., 1996) and detailed in the Supplementary Material.

Dynamic action potential clamp

Our approach is based on the coupling clamp (Tan and Joyner, 1990), model clamp (Wilders et al., 1996), and dynamic clamp (Sharp et al., 1993) techniques. The development of these techniques is built on the concept that an isolated (cardiac) cell can be electrically coupled to either another isolated cardiac cell or to a model analog that mimics the electrical properties of the cardiac myocyte. As diagrammed in Fig. 1, a single cardiac ventricular cell and a transfected HEK-293 cell can be electrically coupled by means of an electrical circuit. The ventricular cell (with I_{Kr} blocked) is in current clamp mode on one patch-clamp setup, whereas the HEK-293 cell is in voltage-clamp mode on another setup. The command potential for the HEK-293 cell is the V_m of the ventricular cell (action potential clamp), and the current input applied to the ventricular cell is the I_{HERG} recorded from the transfected HEK-293 cell, a connection resulting in dAPC condition (Fig. 1 *A*). We performed two kinds of dAPC experiments, defined as the *model-cell mode* and the *real-cell mode*.

Model-cell mode

In model-cell mode (Fig. 1 *B*), the ventricular cell is the Priebe-Beuckelmann (PB) model (Priebe and Beuckelmann, 1998) of a single human ventricular myocyte that is computed in real-time. We extended the model clamp (Wilders et al., 1996) and dynamic clamp (Sharp et al., 1993) techniques,

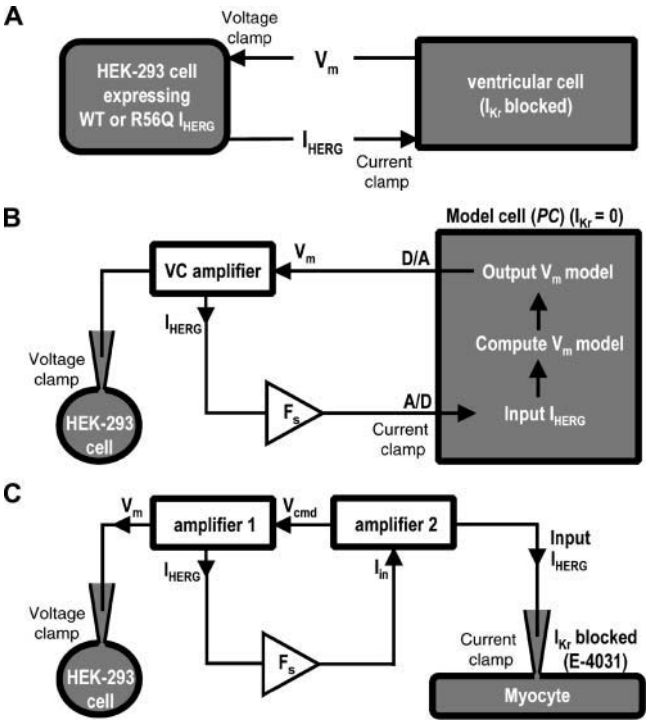

FIGURE 1 Diagram of the dAPC technique used to effectively replace the native I_{Kr} of a ventricular cell with I_{HERG} from a HEK-293 cell. (*A*) Overall experimental design. (*B*) Model-cell mode. I_{HERG} from a HEK-293 cell is recorded, scaled by a factor F_s, and then digitized (*A*/*D*) by a computer (*PC*), which contains a model of the human ventricular cell (Priebe and Beuckelmann, 1998), with $I_{Kr} = 0$. The momentary V_m is computed in real-time using the model equations and the inputted I_{HERG}. The computed V_m is converted into an analog signal (*D*/*A*), sent back to the amplifier, and applied as a voltage-clamp command to the HEK-293 cell. (*C*) Real-cell mode. The model cell has been replaced with a freshly isolated myocyte. I_{HERG} is recorded with amplifier 1, which is voltage-clamp mode, and scaled and applied as external current input (I_{in}) to amplifier 2, which is current clamp mode. The V_m of the myocyte (with I_{Kr} blocked pharmacologically), shaped by the input I_{HERG}, is applied as voltage-clamp command (V_{cmd}) to amplifier 1, thus establishing dAPC.

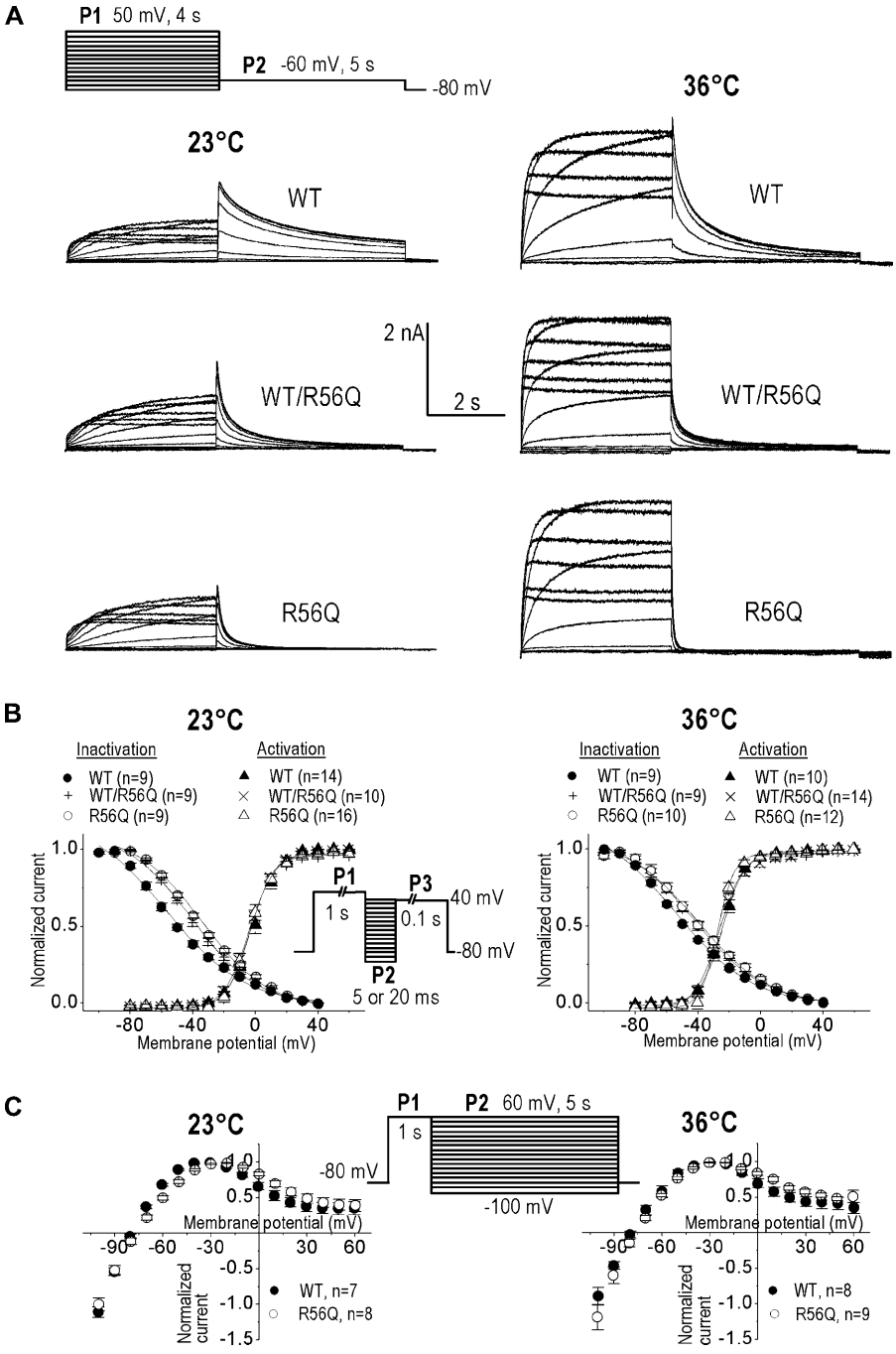

FIGURE 2 Characteristics of WT and R56Q I_{HERG} at 23 and 36°C. (*A*) Representative examples of WT (*top*), WT/R56Q (*middle*), and R56Q (*bottom*) currents elicited by a two-step voltage-clamp protocol. P1-activated I_{HERG}; steady-state current amplitude progressively increased and then decreased with depolarizing voltages, according to voltage-dependent inactivation. P2 elicited I_{HERG} tails; their peak is due to fast recovery from inactivation secondary to repolarization. The subsequent current decline is due to deactivation. (*B*) Voltage dependence of activation (protocol from *A*) and inactivation (protocol from *inset*). See Table 1, for half-maximal (in)activation voltage and slope factor values. (*C*) I-V relationships (peak of I_{HERG} tails during P2 plotted against voltage) of R56Q and WT channels.

implementing dAPC with a real-time Linux operating system (Barabanov and Yodaiken, 1997) as a software platform according to Christini et al. (1999). To attain simultaneous control and recording of V_m and I_{HERG} and to resolve the time-critical tasks of analog-to-digital conversion of I_{HERG}, calculation of the model, and digital-to-analog conversion of V_m, we developed a user program (DynaClamp). This was used with a real-time module that operated on a 1.8-GHz Pentium-4 PC with a 16-bit National Instruments PCI-6052E data acquisition board (National Instruments, Austin, TX) under real-time Linux, and communicated through shared memory and/or first-in, first-out queues. This allows a guaranteed-timing real-time process (i.e., 40-μs periodic time steps with the PB cell model). In all dAPC experiments, I_{Kr} of the model cell is set to zero. We first determine maximal I_{HERG} amplitude in the HEK-293 cell in voltage-clamp configuration, with 4-s depolarizing voltage steps to −10, 0, and 10 mV, from a holding potential of −80 mV, at 36 ± 0.5°C. Considering the unusual kinetics of HERG channels (Lu et al., 2001a), we measure I_{HERG} amplitudes at the end of 4-s pulses rather than from tail current amplitudes. The largest outward current value is then used to estimate the scaling factor (F_s) for the I_{HERG} input to the PB model cell. In our standard protocol, WT as well as R56Q I_{HERG} amplitude are scaled to 47.6 pA (equivalent to the original I_{Kr} amplitude in the PB model). After appropriate scaling, the program establishes dAPC configuration between the model cell and the HEK-293 cell for 10 s, during which a series of 2-ms, 4-nA, 1-Hz suprathreshold stimuli are applied to the computer model cell. The recorded I_{HERG} and computed PB model variables (V_m and ionic currents) and settings

TABLE 1 Parameters of WT, R56Q, and WT/R56Q I_{HERG} activation and inactivation at 23 and 36°C

	23°C			36°C		
	WT	WT/R56Q	R56Q	WT	WT/R56Q	R56Q
Activation						
$V_{1/2}$ (mV)	−1.1 ± 1.1	−2.8 ± 1.1	−3.9 ± 1.0	−26.6 ± 1.4	−28.1 ± 1.0	−28.6 ± 1.4
k (mV)	7.9 ± 0.2	7.9 ± 0.3	7.8 ± 0.2	6.5 ± 0.3	6.3 ± 0.3	6.1 ± 0.3
Inactivation						
$V_{1/2}$ (mV)	−56.6 ± 2.1	−40.4 ± 2.3	−34.5 ± 1.7*	−49.6 ± 2.6	−42.3 ± 3.2	−39.8 ± 3.2*
k (mV)	−24.5 ± 1.5	−22.1 ± 1.5	−22.5 ± 1.5	−23.5 ± 0.5	−22.8 ± 0.7	−23.1 ± 1.0

*$P < 0.05$ for R56Q versus WT. Values are mean ± SE; for n, the number of experiments, see Fig. 2 *B*.

of the DynaClamp program are stored on disk for off-line analysis. The time-dependent changes in V_m of the ventricular model cell are derived from WT and/or mutant I_{HERG} input and the model equations. The combination of the cell model and WT I_{HERG} will then result in a normal AP. Using the same method for HEK-293 cells with mutant channels will reveal an AP, which resembles the ventricular AP of the patient from which the mutant was derived.

Real-cell mode

In real-cell mode, the model cell is replaced with a rabbit left-ventricular myocyte (Fig. 1 *C*). The procedure to define F_s is as follows: we measure I_{HERG} amplitude in the HEK-cell (as described above) and, simultaneously, estimate I_{Kr} density in the rabbit cell (as E-4031 sensitive current). We elicite APs in the myocyte at 1 Hz in the presence of E-4031, and then establish coupling between the myocyte and the HEK-293 cell, implementing scaled WT I_{HERG}. A proper F_s value would result in I_{HERG} density comparable to that of the I_{Kr} density in the myocyte and in a typical AP duration at 90% repolarization (APD_{90}) value of 230.8 ± 4.5 ms at 1 Hz (see Table 2 in Supplementary Material), characteristic for these cells. Ca^{2+} loading of the myocytes exhibiting long action potentials in the presence of E-4031 (as in Fig. 8 *B*) is likely. However, this process loses its grip when the scaled I_{HERG} is implemented and APD is shortened to its initial value (to same APD as before the addition of E-4031) where Ca^{2+} loading will be ruled out.

In both real-cell and model-cell modes, we can apply various stimulation rates; V_m of the ventricular cell and I_{HERG} of HEK-293 cell are displayed on-

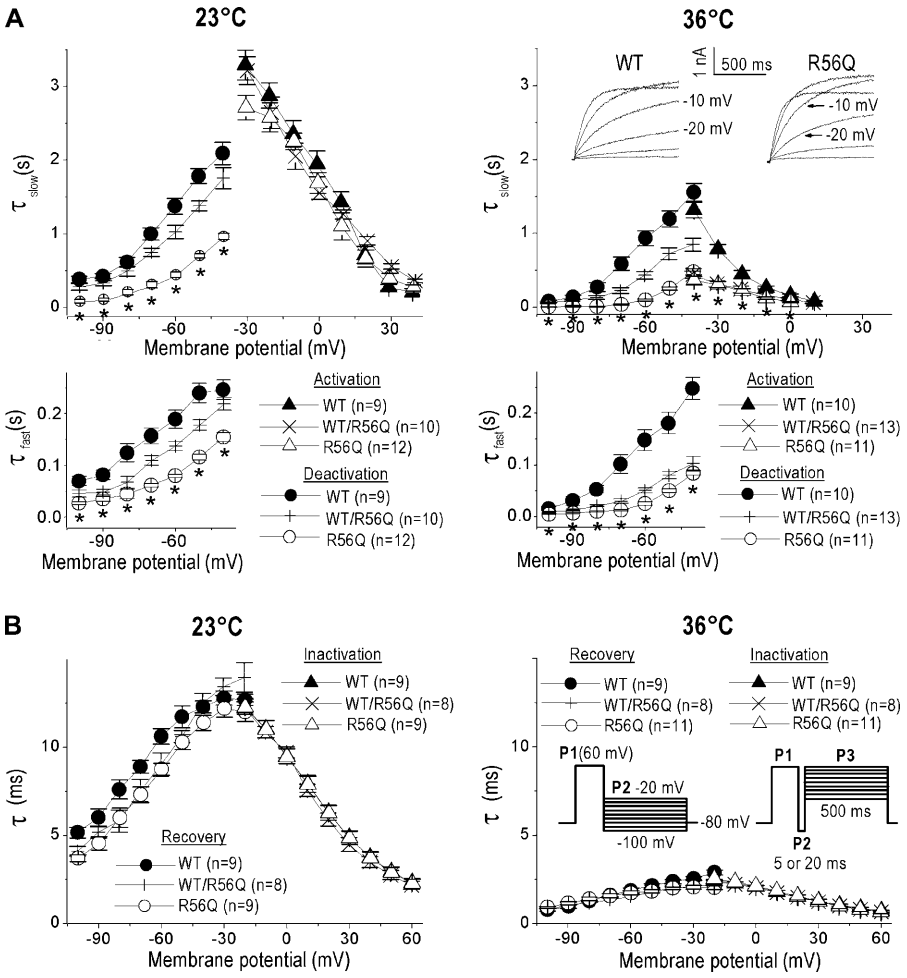

FIGURE 3 Time constants of WT and R56Q I_{HERG} kinetics at 23 and 36°C. (*A*) Time constant of activation (τ_{slow}, *triangles*) and fast and slow time constant of deactivation (τ_{fast} and τ_{slow}, *circles*). Voltage-clamp protocols are shown in Fig. 2, *A* and *C*, respectively, and described in the Supplementary Material. Faster activation of R56Q HERG channels was apparent only at 36°C (see *current traces inset*), whereas deactivation was faster for R56Q than for WT at both 23 and 36°C (*, significant difference for R56Q versus WT, $P < 0.05$). WT/R56Q showed a mixed phenotype. (*B*) Time constants of inactivation (*triangles*) and recovery from inactivation (*circles*). Voltage-clamp protocols are shown as insets and described in the Supplementary Material.

line, thus providing instant information on the dAPC. DynaClamp allows scaling of the input current to any desired magnitude and subtraction of artifacts (e.g., endogenous HEK-293 cell currents), before I_{HERG} is applied to the ventricular cell. Leak subtraction, however, was not necessary as I_{HERG}-downscaling already reduced endogenous currents to negligible levels.

Statistics

Data are expressed as mean ± SE (n, number of cells) and considered significantly different if $P < 0.05$ in ANOVA and Student's t-test.

RESULTS

Electrophysiological characterization of WT, R56Q, and WT/R56Q HERG channels

To investigate the influence of recording temperature and expression system on the WT and R56Q HERG channel kinetics, we performed a series of voltage-clamp experiments at both 23°C and 36°C. We also coexpressed WT and R56Q cDNAs, in analogy to what is presumed to be present in a patient with a single WT and mutant allele. Fig. 2 shows typical WT and/or R56Q I_{HERG} expressed in HEK-293 cells. Increasing the recording temperature resulted in several changes, including faster I_{HERG} time course and larger amplitudes (Fig. 2 *A*), and a negative shift in the voltage dependence of activation (Fig. 2 *B*, Table 1). The R56Q mutation caused a positive shift in the voltage dependence of steady-state channel availability at both 23°C and 36°C (Fig. 2 *B*, Table 1). The normalized current-voltage (I-V) relationships remained unchanged (Fig. 2 *C*). At 36°C, the mean densities of I_{HERG}, measured at the end of a 4-s pulse to −20 mV, were 269 ± 42 and 243 ± 49 pA/pF with WT ($n = 17$) and R56Q channels ($n = 15$), respectively (not significantly different).

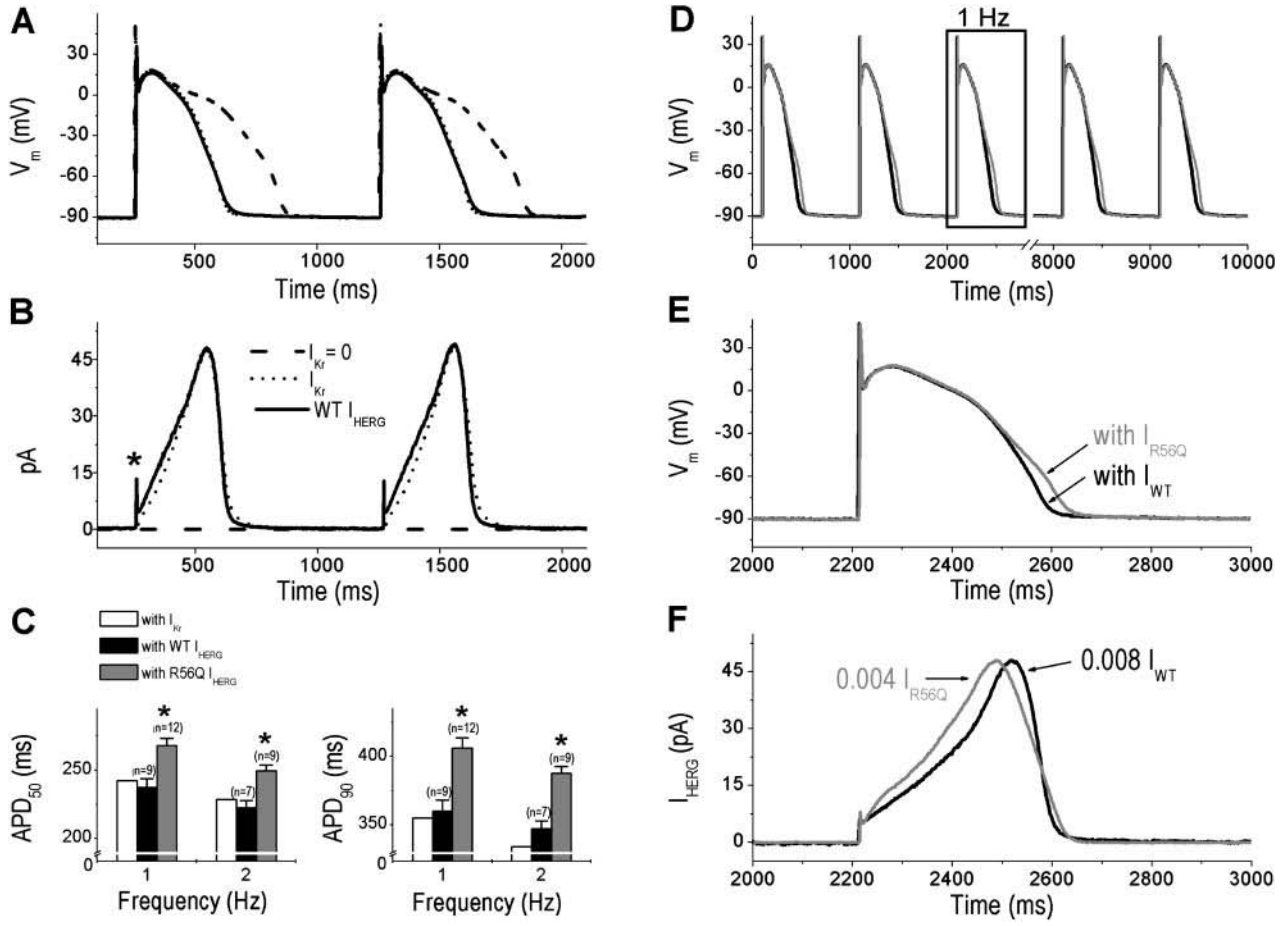

FIGURE 4 The dAPC experiment with WT and R56Q I_{HERG} replacing I_{Kr} in the PB model cell. (*A*) WT I_{HERG} is an effective substitute for I_{Kr}. Superimposed APs (at 1 Hz) in the absence of I_{Kr} (*long dashed line*), with I_{Kr} (*short dashed line*), or with WT I_{HERG} (*solid line*, $I_{Kr} = 0$). (*B*) Time course of the AP waveform-elicited WT I_{HERG} is similar to that of I_{Kr} in the PB cell model except for the early activation (*asterisk*) phase. F_s for I_{HERG} was 0.008; see text for details. (*C*) APD_{50} and APD_{90} values at 1 and 2 Hz (*, significant difference for R56Q versus WT). (*D*) Representative APs with WT I_{HERG} (*solid line*) or R56Q I_{HERG} (*shaded line*), at 1 Hz ($I_{Kr} = 0$). (*E* and *F*) Boxed APs from *D* (*E*) and associated I_{HERG} (*F*) on an expanded timescale. The HERG currents were scaled to identical maximal amplitude values (F_s values indicated) and applied to the PB model cell as an external current input, and are thus responsible for repolarization of the model cell.

Time constants of I_{HERG} kinetics showed marked temperature dependence (Fig. 3). At 36°C, the time course of R56Q channel activation was approximately threefold faster at all voltages than that of WT channels (Fig. 3 *A*; and see Table 1 in the Supplementary Material). For the heteromultimer WT/R56Q, the activation time constants were identical to those of R56Q alone. Remarkably, in *Xenopus* oocytes, the time course of R56Q channel activation was shown to be slower than for those of WT channels (Chen et al., 1999). The deactivation time course of R56Q channels was markedly faster than for those of WT at both temperatures, as shown by the diminution of both (fast and slow) time constants (Fig. 3 *A*; and see Table 1 in the Supplementary Material). The finding that the mutation causes faster deactivation is in agreement with the results of Chen et al. (1999). Time constants of inactivation and recovery from inactivation (Fig. 3 *B*) did not differ significantly between WT and R56Q (see Table 2 in the Supplementary Material). Our results demonstrate that acceleration of the R56Q HERG activation remains obscured at 23°C and highlight the importance of investigating HERG kinetics at physiological temperature.

Replacing I_{Kr} of the model cell with WT and R56Q I_{HERG}

In the comprehensive human subepicardial ventricular cell model by Priebe and Beuckelmann (1998), description of I_{Kr} is based on data from human ventricular cells (Li et al., 1996). With model-cell I_{Kr} set to zero, the AP prolongs (Fig. 4 *A*). When WT I_{HERG} from a HEK-293 cell replaces I_{Kr}, AP characteristics are restored and the AP can be considered as normal (Fig. 4, *A* and *C*). Similar results were obtained when the KCl content of the Tyrode solution was modified to 5.4 mmol/L (see, in Supplementary Material, Fig. 1 and Table 3). The time course of the scaled I_{HERG} compares well to that of I_{Kr} of the model cell (Fig. 4 *B*) except that the initial time course of I_{HERG} differs from that of the mathematically described I_{Kr}, which is due to the model assumption that I_{Kr} inactivation is instantaneous. Many HERG channels are still in the open state at −90 mV as a result of slow deactivation (Lu et al., 2001a), and this results in an initial transient peak (*asterisk*), reflecting the sudden increase of the electrochemical driving force for K^+ during the AP upstroke. After a fast decay of the transient peak amplitude, caused by inactivation during the overshoot of the AP and by the decreasing driving force for K^+ at less depolarized V_m, current increases progressively as channels rapidly recover from inactivation, a process faster than the deactivation (Sanguinetti et al., 1995; Trudeau et al., 1995; Smith et al., 1996; Zhou et al., 1998). With repolarization progressing, HERG channels dwell in a highly stable open state before closing (Wang et al., 1998), resulting in a resurgent current. Altered HERG channel properties in long-QT syndrome generally reduce the magnitude of this resurgent current

TABLE 2 Relative densities of selected ionic currents in the subendocardial, *M*, and subepicardial cell models

Current	Subendocardial	Midmyocardial (*M*)	Subepicardial
I_{to}	25%; Näbauer et al. (1996)	87%; Liu et al. (1993)	100%
I_{Ks}	92%; Liu and Antzelevitch (1995)	46%; Liu and Antzelevitch (1995)	100%
I_{K1}	89%; Liu et al. (1993)	74%; Liu et al. (1993)	100%

All densities are percentage relative to the standard densities in the PB model that essentially describes a human subepicardial ventricular myocyte (Conrath et al., 2004).

(Chen et al., 1999; Sanguinetti et al., 1996). Both I_{Kr} and I_{HERG} reach maximum value ~−40 mV, then rapidly deactivate in a time- and voltage-dependent manner.

To study the functional consequences of the R56Q mutation, we performed dAPC experiments with the PB cell model and WT and/or mutant I_{HERG} from the HEK-293 cell, in model-cell mode (Fig. 4 *D*). Results of these experiments, remarkably consistent with the role of HERG channels in cardiac repolarization, clearly show that the AP is prolonged by the altered I_{HERG} kinetics of the mutant (Fig. 4, *C–E*; see also Table 3 in the Supplementary Material). The WT or R56Q I_{HERG}, scaled to identical maximal amplitude values (Fig. 4 *F*, F_s values indicated), was added to the PB model cell as an external current input, and thus contributed to repolarization of the model cell. Consistent with the results of voltage-clamp experiments at 36°C, the input WT and R56Q I_{HERG} have different initial and late phases. Apparently, mutant I_{HERG} is initially larger than the WT. The faster

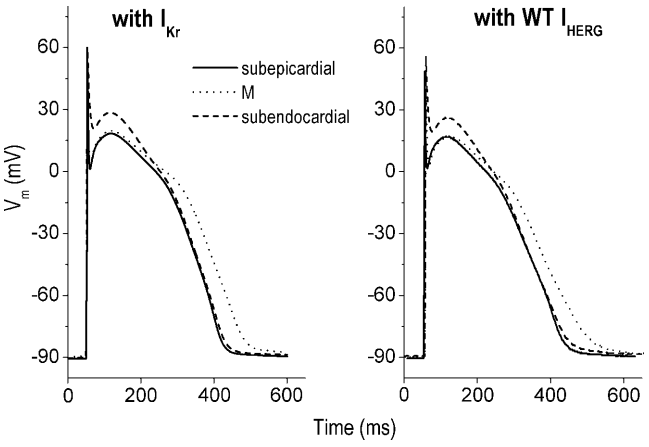

FIGURE 5 Regional AP heterogeneity is reproduced in a dAPC experiment. Subepicardial, *M*, and subendocardial APs were simulated at 1 Hz; note the different plateau levels and repolarization phases in these model cells (see the modified current densities in Table 2).

onset of the R56Q I_{HERG} decay indicates faster deactivation for R56Q HERG channels.

Action potential heterogeneity in the PB model cell with WT and R56Q I_{HERG}

The heterogeneity of the electrical properties of the myocytes in the different layers of the human left ventricle is now well established. As in our previous model studies (Bernus et al., 2002; Conrath et al., 2004), we generated subendocardial, midmyocardial (*M*), and subepicardial model cells by adjusting selected membrane ionic currents in the PB model cell (Table 2). When, in a dAPC experiment, WT I_{HERG} replaced model-cell I_{Kr}, APs of different shape and duration could still be reproduced (Fig. 5). The major consequence of the R56Q mutation on the AP characteristics of these cell types was AP prolongation (Fig. 6). We analyzed in detail AP characteristics of the epicardial model cell (Fig. 7), comparing the frequency dependence of APD_{90} values generated with model-cell I_{Kr} to values obtained with WT or R56Q I_{HERG}. These values are comparable when WT I_{HERG} replaces I_{Kr}, whereas R56Q I_{HERG} causes frequency-dependent APD_{90} prolongation (Fig. 7 *A*). APD_{90} with the cotransfected WT/R56Q channels showed intermediate values (not shown). The role of WT or R56Q I_{HERG} in shaping the AP was evaluated by phase plane analysis (Sperelakis and Shumaker, 1968), plotting membrane currents against membrane potential (Fig. 7 *B*). With input I_{HERG} scaled for identical amplitudes for both WT and R56Q, the consequence of the mutation is apparent. The

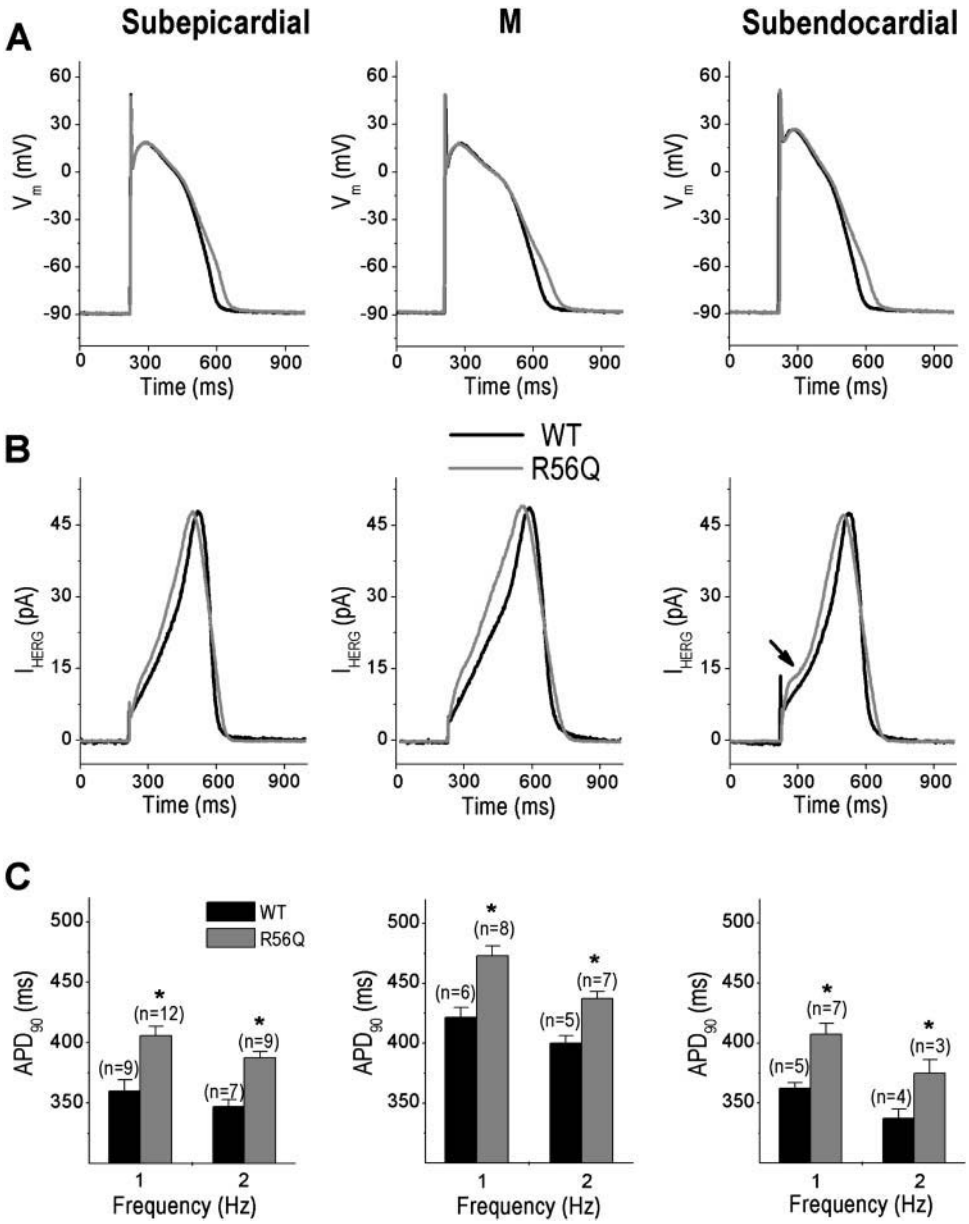

FIGURE 6 AP prolongation caused by the R56Q mutation in the three different cell types of Fig. 5. (*A*) Representative APs and (*B*) the corresponding I_{HERG}; note the increased inactivation of R56Q I_{HERG} (*arrow*) at the positive plateau-voltages of the subendocardial cell; (*C*) averaged APD_{90} values at 1 and 2 Hz (*, significant difference for R56Q versus WT I_{HERG}).

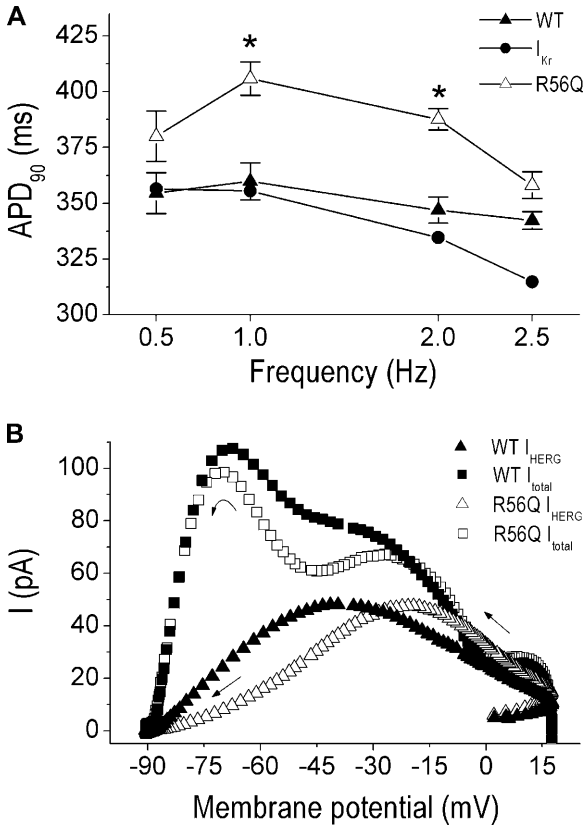

FIGURE 7 AP characteristics of the subepicardial PB model cell. (*A*) Frequency dependence with I_{Kr}, WT I_{HERG} ($n = 10$), or R56Q I_{HERG} ($n = 8$) (*, significant difference for R56Q versus WT). (*B*) Phase-plane plot for the net membrane current (I_{total}) and I_{HERG} during repolarization (starting from ~+18 mV during phase-1 repolarization). APs from which these phase planes were obtained were generated at 1 Hz and are shown in Fig. 4, *D* and *E*. Arrows indicate progression of time.

most notable changes are detected during phase-3 repolarization, with a reduction of the net membrane current (I_{total}).

Replacing I_{Kr} of a rabbit ventricular cell with WT and R56Q I_{HERG}

Results with I_{HERG} replacing I_{Kr} in the model cell show that the overall properties of the AP are well reproduced in a dAPC experiment (Figs. 4 *A* and 5). Next, we used the real-cell variant of the technique (Fig. 8). Ionic currents underlying APs of a rabbit ventricular cell are comparable with those in a human ventricular cell. Fig. 8 *A* shows typical whole-cell currents during 4-s depolarizing prepulses to 0 mV and tail currents after returning to −60 mV. I_{Kr} may be differentially expressed in rabbit ventricles (Cheng et al., 1999), thus we first demonstrate I_{Kr} presence as the E-4031 sensitive current (Clay et al., 1995). Currents during depolarization as well as tails were markedly diminished in the presence of E-4031, resulting in prolonged repolarization and early after-depolarizations in all cells tested ($n = 9$) (Fig. 8 *B*). dAPC experiments ($n = 5$) were performed with a single myocyte coupled first to a HEK-293 cell with WT I_{HERG} (Fig. 8 *C*), and then to a HEK-293 cell with R56Q I_{HERG} (Fig. 8 *D*). In both cases, AP parameters were determined at different stimulation frequencies (Fig. 9; see also Table 4 in the Supplementary Material). The measured resting V_m of the myocytes was −82.9 ± 2.7 mV. APs were effectively reconstituted in a dAPC experiment with WT I_{HERG}. APs with R56Q I_{HERG} exhibited significant APD prolongation at 0.2 and 1 Hz (Fig. 9 *B*). These experiments also revealed that WT I_{HERG} consists of an early fast transient outward current followed by a sustained outward current (Figs. 8 *C* and 9). Transient I_{HERG} may contribute importantly to AP dynamics during tachycardia (Lu et al., 2001a). Amplitude of the transient component showed positive frequency dependence (Fig. 9 *C*), whereas that of the sustained component peaked during the terminal AP repolarization, in a reverse frequency-dependent manner between 1 and 5 Hz (Fig. 9 *D*). Although frequency dependence of the sustained R56Q I_{HERG} was similar to that of WT I_{HERG}, frequency dependence of the R56Q I_{HERG} transient component was absent, consistent with the impaired deactivation kinetics of these channels.

DISCUSSION

A broad agreement prevails on the role of HERG channels in AP repolarization. For a better understanding of the link between LQT2 mutations and the inherent clinical phenotype, insight into the nature of HERG channel (dys)function is indispensable. As a longstanding approach, the time- and voltage-dependence of the HERG channel has most frequently been characterized using stepwise voltage-clamp protocols, and description of the HERG current was often based on the extrapolation of results obtained in various heterologous expression systems. However, it is becoming clear that complex features of HERG channel kinetics during the cardiac AP can best be studied during physiological voltage waveforms (Hancox et al., 1998; Lu et al., 2001a; Zhou et al., 1998) and, as shown in the present study, even better during dAPC condition (i.e., by letting them shape the ventricular action potential), in line with their normal function.

The NH_2 terminus of the α-subunit of the channel regulates deactivation gating and represents a mechanism by which functional diversity is generated in HERG and related channels (Wang et al., 1998). Our electrophysiological experiments demonstrate that the R56Q mutation impairs not only deactivation (Chen et al., 1999) but activation kinetics as well, the latter becoming apparent only at 36°C (Fig. 3 *A*). Intriguingly, a faster activation and a positive shift in the voltage dependence of channel availability (Fig. 2 *B*), would actually act to shorten AP duration. Characteristics of the heteromultimeric (WT/R56Q) channels suggest that some of the functional effects

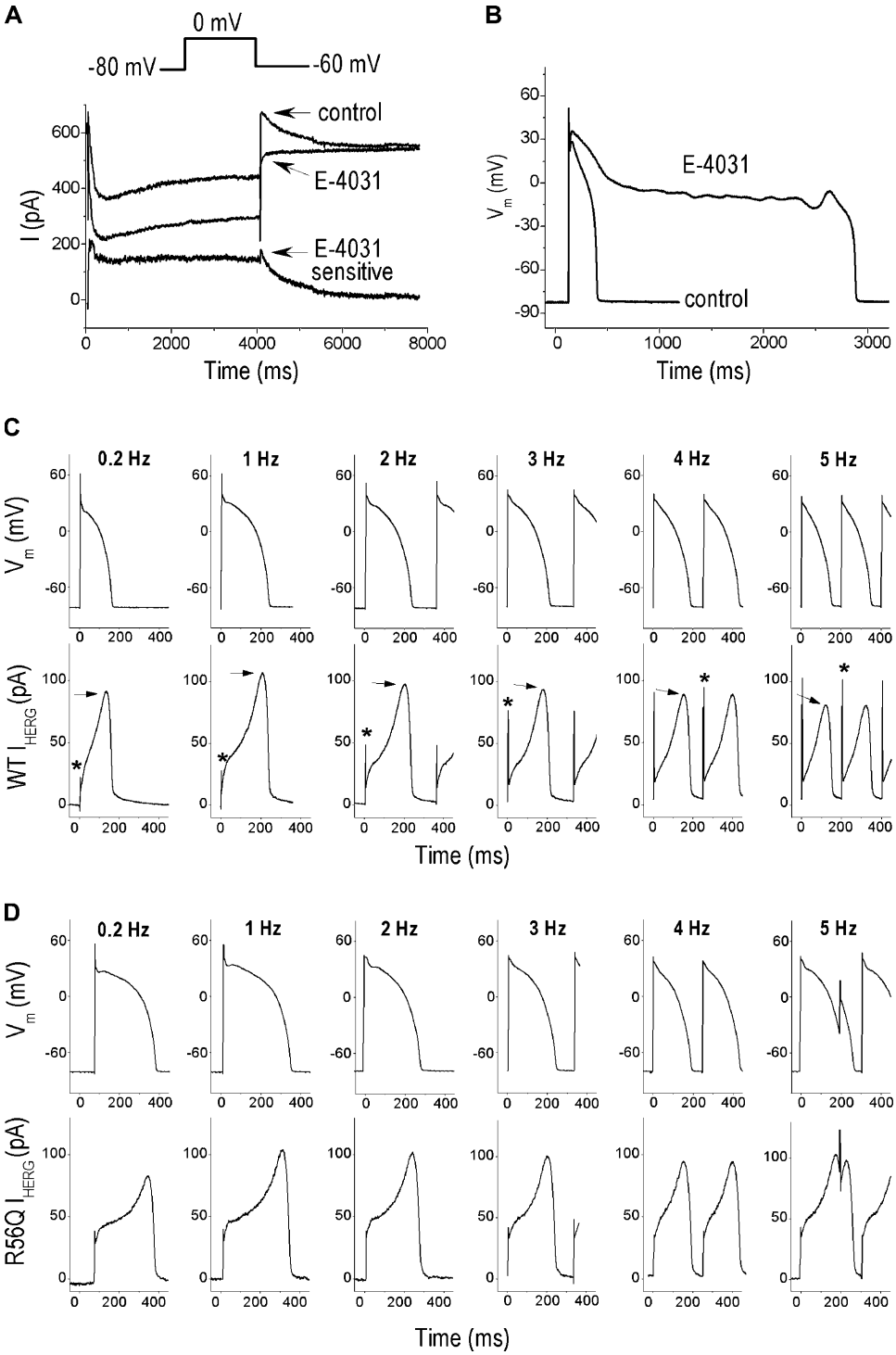

FIGURE 8 The dAPC experiment with I_{HERG} replacing I_{Kr} in rabbit myocytes. (*A*) Block of I_{Kr} with 5 μmol/L E-4031 (*inset*, pulse protocol). Superimposed tracings of typical recordings in absence (*control*) and presence of E-4031, and difference (*E-4031 sensitive*) current. Mean I_{Kr} density, determined from the E-4031 sensitive current, was 0.63 ± 0.1 pA/pF ($n = 9$). (*B*) APs in a myocyte stimulated at 0.2 Hz before and after applying E-4031. Superfusion of cells with E-4031 caused early after-depolarizations. (*C* and *D*) APs from a myocyte and associated WT (*C*) or R56Q I_{HERG} (*D*) at different frequencies. The myocyte was successively coupled to HEK-293 cells transfected with WT or R56Q HERG channels. Note the different I_{HERG} waveforms (*, transient I_{HERG}; *arrow*, sustained I_{HERG}) and frequency-dependent AP prolongation with R56Q (see also Table 2 in the Supplementary Material).

are not simply combined, but that a dominant negative interaction can also occur between the WT and R56Q HERG channels (see activation time constants at 36°C in Fig. 3 *A*). Along the same lines with the impaired biophysical properties, certain mutations in the Per-Arnt-Sim domain might actually cause an HERG protein trafficking defect (Paulussen et al., 2002). However, we did not find significant differences in I_{HERG} densities of WT and/or R56Q channels, suggesting that the primary defect in mutant channel properties is attributable to altered gating.

MinK-related peptide (MiRP1)/HERG complexes have received considerable support as molecular correlates for native I_{Kr} (Abbott et al., 1999, 2001). We did not coexpress MiRP1 for reconstitution of native I_{Kr} by HERG, as

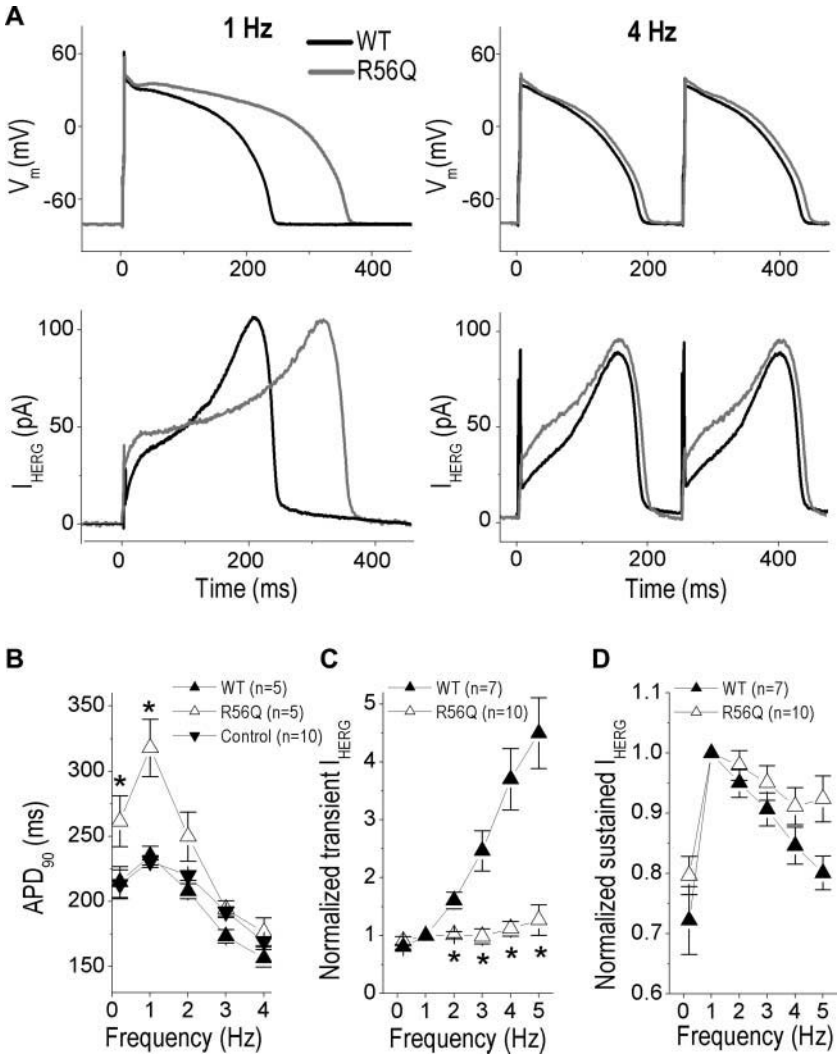

FIGURE 9 Action potential characteristics of rabbit ventricular myocytes with WT and R56Q I_{HERG}. (*A*) Superimposed APs from a single myocyte successively coupled to HEK-293 cells expressing WT (*solid line*) or R56Q I_{HERG} (*shaded line*), and the corresponding I_{HERG} waveforms at 1 and 4 Hz. (*B–D*) Frequency dependence of APD_{90} prolongation (*B*; see also Table 2 in the Supplementary Material) and transient (*C*) and sustained (*D*) I_{HERG} amplitudes, each normalized to their values at 1 Hz. Asterisks indicate significant difference for R56Q versus WT.

properties of I_{HERG} in mammalian systems are similar in many ways to those of native I_{Kr}, and discrepancies that remain cannot be fully abolished by coexpression with MiRP1 (Weerapura et al., 2002).

Most experimental data on cardiac ion channel (dys)function have been obtained in expression systems, away from the cellular environment where these channels function to generate the cardiac action potential. Table 3 shows a comparison of I_{Kr} in the various systems: 1), PB model; 2), human ventricle; 3), rabbit ventricle; and 4), HEK-293 cells. The relatively few studies of human ventricular I_{Kr} make it difficult to fully validate such comparison. Nevertheless, the study of Iost et al. (1998) provides data on I_{Kr} in human ventricular tissue obtained from healthy patients not receiving medication. Despite the apparent differences between some properties of I_{HERG} and I_{Kr} in the present study and previous results in the literature, mammalian cell lines generally provide an adequate environment for HERG channels. Here, experiments should be performed at physiological temperatures, as HERG channel gating at 36°C more closely resembles endogenous I_{Kr} (Zhou et al, 1998; this study). Necessarily, the *Xenopus* system can be an alternative when channels do not express well in a mammalian cell line, although 36°C for oocytes is not physiological, and observed differences in the behavior of the expressed cardiac potassium channel proteins suggest that endogenous factors in oocytes dictate channel properties to some extent (Seebohm et al., 2001).

We have introduced the dAPC technique to investigate AP characteristics in ventricular myocytes, by replacing I_{Kr} in these cells by WT or mutant I_{HERG} generated in HEK-293 cells. In both model-cell and real-cell modes, frequency dependence of the APDs was comparable when WT I_{HERG} replaced I_{Kr}. AP characteristics of the ventricular cells were effectively reproduced by WT I_{HERG}, whereas the R56Q I_{HERG} caused a frequency-dependent increase in APD.

Superimposed phase plane plots of the repolarization phases of model-cell APs indicate that the net membrane current is severely affected by the mutation during the late repolarization phase. APD_{90} values with R56Q I_{HERG} were

TABLE 3 Biophysical properties of I_{Kr} (in the PB ventricular model cell or in freshly isolated myocytes) and I_{HERG} (transiently expressed in HEK-293 cells)

	$I_{density}$ (pA/pF)	Activation	Inactivation	Deactivation	References
Model I_{Kr}	0.31				Priebe and Beuckelmann (1998); This study
$V_{1/2}$ (mV)		−21.0	−26.0		
k (mV)		5.4	−23.0		
τ (ms)		194.5 (+50 mV)		494.2 (−40 mV)	
Human I_{Kr}	~0.3				Li et al. (1996); Iost et al. (1998)
$V_{1/2}$ (mV)		−14.0 ± 4, −5.7*†	ND		
k (mV)		7.7 ± 2.7, 5.6*	ND		
τ (ms)		192.0 ± 53 (+50 mV)		600.0 ± 54 (−40 mV)*	
Rabbit I_{Kr}	0.3, 0.6‡				Lu et al. (2001b); This study
$V_{1/2}$ (mV)		−21.9	ND		
k (mV)		ND	ND		
τ_1 (ms)		78.0 ± 4 (+50 mV)		119.0 ± 25 (−50 mV)	
τ_2 (ms)		624.0 ± 42 (+50 mV)		569.0 ± 123 (−50 mV)	
WT I_{HERG}	269 ± 42				Zhou et al. (1998); This study
$V_{1/2}$ (mV)		−25.9 ± 2.0§, −26.6 ± 1.4	−49.6 ± 2.6		
k (mV)		6.0 ± 0.3§, 6.5 ± 0.3	−23.5 ± 0.5		
τ_1 (ms)		18.0 ± 3.0 (+40 mV)§		180.0 ± 20§ (−40 mV)	
τ_2 (ms)				1299 ± 118§ (−40 mV)	

Values are mean ± SE; *ND*, not determined. All experiments were done under comparable conditions: 34–37°C, extracellular K^+ concentration = 4–6 mmol/L, extracellular divalent cation concentration = 2–3 mmol/L. Current density ($I_{density}$) was defined as current level at the end of a −20 mV depolarizing pulse normalized to cell capacitance.

*Iost et al. (1998).

†Note that Iost et al. (1998) did not mention any correction for liquid junction potential (*LJP*). Taking into account an LJP of ~−10 mV under the given ionic conditions (Barry and Lynch, 1991), the actual $V_{1/2}$ would be −16 mV.

‡This study.

§Zhou et al. (1998)

increased at lower stimulation rates and unchanged at higher frequencies. Consistent with the role of HERG in the suppression of arrhythmias initiated by premature beats (Lu et al., 2001a), the technique revealed the presence of an early fast, frequency-dependent transient WT I_{HERG}. The frequency-dependent increase of this current component was absent with R56Q channels. APs with R56Q I_{HERG} were generally longer (Fig. 9 *B*), which can be explained by the faster deactivation. However, the reason why the faster activating, thus initially larger R56Q I_{HERG} does not have significant effect on the AP plateau is less obvious. It is likely that the faster activation of the R56Q I_{HERG} in the myocyte causes a slightly modified membrane potential in the early plateau phase of the AP, influencing activation of other currents. Computer simulations using either the PB model or the recently published human ventricular cell model by Ten Tusscher et al. (2004) also predict little or no effect of a moderate increase in I_{Kr} during the plateau phase of the action potential (data not shown). On the other hand, even small changes of the myocyte's membrane potential can cause significant changes in activation of voltage-dependent currents, such as the transient outward current, I_{to} (Greenstein et al., 2000) and calcium current, I_{Ca} (Fülöp et al., 2003).

In summary, both the computed model of the human ventricular cell as well as a freshly isolated myocyte can effectively be used in dAPC experiments. Kinetic features that are difficult to investigate with standard voltage-clamp protocols become apparent with the dAPC technique. The model-cell mode offers an outstanding reproducibility of the results during experimentation, as the input WT or mutant I_{HERG} is the only variable. However, the technically more difficult real-cell mode can reveal AP waveforms and I_{HERG} kinetics that can be considered truly physiological. Additionally, the real-cell mode offers the advantage that stimulation rates above 2.5 Hz (maximal value in the model cell) can easily be achieved. Theoretically, any individual conductance in the model cell or in a real ventricular cell (if a specific blocker for the investigated conductance is available) can be replaced by a surrogate input current from an expression system.

In the model-cell variant of the technique, it is a straightforward operation to test the effect of interventions directed at counteracting the effects of the mutations in HERG, e.g., increasing the slow repolarizing component (I_{Ks}) of the delayed rectifier K^+ current.

Data presented here on the behavior of WT and R56Q HERG channels may have implications for further studies, where differences between WT and mutant channels are subtle. With our approach, the contribution of (mutated) channels to the AP is determined without making assumptions with regard to the kinetic properties of the channels, and the altered shape of AP directly reflects the effect of the

mutation. The dAPC technique allows other cardiac ion channels than HERG (e.g., SCN5A, KvLQT1) to be studied as well.

General considerations

The inherent limitations of the PB model and of simulations when creating transmural AP heterogeneity on the basis of experimental findings have been discussed before (Bernus et al., 2002; Priebe and Beuckelmann, 1998). During dAPC experiments, in both model-cell and real-cell modes, we assumed that the defect in the R56Q channel is attributed to altered gating. Accordingly, we scaled WT and mutant input I_{HERG} to similar magnitudes.

We are aware that it is potentially conceivable that a mutation in an ion channel gene could result in compensatory changes in other ion channel genes in vivo, representing a general limitation of any heterologous expression system. Short-term alteration of mRNA levels of ion channels, caused by rapid pacing, is well documented (Yamashita et al., 2000). Libbus et al. (2004) provide direct evidence for I_{to} remodeling in the ventricle caused by reduced AP upstroke amplitude, on a surprisingly short timescale.

SUPPLEMENTARY MATERIAL

An online supplement to this article can be found by visiting BJ Online at http://www.biophysj.org.

This work was supported by Netherlands Heart Foundation grant No. 2001B155.

REFERENCES

Abbott, G. W., S. A. Goldstein, and F. Sesti. 2001. Do all voltage-gated potassium channels use MiRPs? *Circ. Res.* 88:981–993.

Abbott, G. W., F. Sesti, I. Splawski, M. E. Buck, M. H. Lehmann, K. W. Timothy, M. T. Keating, and S. A. Goldstein. 1999. MiRP1 forms I_{Kr} potassium channels with HERG and is associated with cardiac arrhythmia. *Cell.* 97:175–187.

Barabanov, M., and V. Yodaiken. 1997. Introducing real-time Linux. *Linux J.* 34:19–23.

Barry, P. H., and J. W. Lynch. 1991. Liquid junction potentials and small cell effects in patch-clamp analysis. *J. Membr. Biol.* 121:101–117.

Bernus, O., R. Wilders, C. W. Zemlin, H. Verschelde, and A. V. Panfilov. 2002. A computationally efficient electrophysiological model of human ventricular cells. *Am. J. Physiol. Heart Circ. Physiol.* 282:H2296–H2308.

Chen, J., A. Zou, I. Splawski, M. T. Keating, and M. C. Sanguinetti. 1999. Long QT syndrome-associated mutations in the Per-Arnt-Sim (PAS) domain of HERG potassium channels accelerate channel deactivation. *J. Biol. Chem.* 274:10113–10118.

Cheng, J., K. Kamiya, W. Liu, Y. Tsuji, J. Toyama, and I. Kodama. 1999. Heterogeneous distribution of the two components of delayed rectifier K^+ current: a potential mechanism of the proarrhythmic effects of methanesulfonanilide Class III agents. *Cardiovasc. Res.* 43:135–147.

Christini, D. J., K. M. Stein, S. M. Markowitz, and B. B. Lerman. 1999. Practical real-time computing system for biomedical experiment interface. *Ann. Biomed. Eng.* 27:180–186.

Clancy, C. E., and Y. Rudy. 2001. Cellular consequences of HERG mutations in the long QT syndrome: precursors to sudden cardiac death. *Cardiovasc. Res.* 50:301–313.

Clay, J. R., A. Ogbaghebriel, T. Paquette, B. I. Sasyniuk, and A. Shrier. 1995. A quantitative description of the E-4031-sensitive repolarization current in rabbit ventricular myocytes. *Biophys. J.* 69:1830–1837.

Conrath, C. E., R. Wilders, R. Coronel, J. M. De Bakker, P. Taggart, J. R. De Groot, and T. Opthof. 2004. Intercellular coupling through gap junctions masks *M* cells in the human heart. *Cardiovasc. Res.* 62:407–414.

Curran, M. E., I. Splawski, K. W. Timothy, G. M. Vincent, E. D. Green, and M. T. Keating. 1995. A molecular basis for cardiac arrhythmia: HERG mutations cause long QT syndrome. *Cell.* 80:795–803.

Fülöp, L., T. Bányász., J. Magyar, N. Szentandrássy, A. Varró, and P. P. Nánási. 2003. Reopening of L-type calcium channels in human ventricular myocytes during applied epicardial action potentials. *Acta Physiol. Scand.* 179:1–9.

Greenstein, J. L., R. Wu, S. Po, G. F. Tomaselli, and R. L. Winslow. 2000. Role of the calcium-independent transient outward current I_{to1} in shaping action potential morphology and duration. *Circ. Res.* 87:1026–1033.

Hancox, J. C., A. J. Levi, and H. J. Witchel. 1998. Time course and voltage dependence of expressed HERG current compared with native ''rapid'' delayed rectifier *K* current during the cardiac ventricular action potential. *Pflugers Arch.* 436:843–853.

Iost, N., L. Virág, M. Opincariu, J. Szécsi, A. Varró, and J. G. Papp. 1998. Delayed rectifier potassium current in undiseased human ventricular myocytes. *Cardiovasc. Res.* 40:508–515.

Li, G. R., J. Feng, L. Yue, M. Carrier, and S. Nattel. 1996. Evidence for two components of delayed rectifier K^+ current in human ventricular myocytes. *Circ. Res.* 78:689–696.

Libbus, I., X. Wan, and D. S. Rosenbaum. 2004. Electrotonic load triggers remodeling of repolarizing current I_{to} in ventricle. *Am. J. Physiol. Heart Circ. Physiol.* 286:H1901–H1909.

Liu, D. W., and C. Antzelevitch. 1995. Characteristics of the delayed rectifier current (I_{Kr} and I_{Ks}) in canine ventricular epicardial, mid-myocardial, and endocardial myocytes. A weaker I_{Ks} contributes to the longer action potential of the *M* cell. *Circ. Res.* 76:351–365.

Liu, D. W., G. A. Gintant, and C. Antzelevitch. 1993. Ionic bases for electrophysiological distinctions among epicardial, midmyocardial, and endocardial myocytes from the free wall of the canine left ventricle. *Circ. Res.* 72:671–687.

Lu, Y., M. P. Mahaut-Smith, A. Varghese, C. L. Huang, P. R. Kemp, and J. I. Vandenberg. 2001a. Effects of premature stimulation on HERG K^+ channels. *J. Physiol.* 537:843–851.

Lu, Z., K. Kamiya, T. Opthof, K. Yasui, and I. Kodama. 2001b. Density and kinetics of I_{Kr} and I_{Ks} in guinea pig and rabbit ventricular myocytes explain different efficacy of I_{Ks} blockade at high heart rate in guinea pig and rabbit: implications for arrhythmogenesis in humans. *Circulation.* 104:951–956.

Marbán, E. 2002. Cardiac channelopathies. *Nature.* 415:213–218.

Näbauer, M., D. J. Beuckelmann, P. Uberfuhr, and G. Steinbeck. 1996. Regional differences in current density and rate-dependent properties of the transient outward current in subepicardial and subendocardial myocytes of human left ventricle. *Circulation.* 93:168–177.

Paulussen, A., A. Raes, G. Matthijs, D. J. Snyders, N. Cohen, and J. Aerssens. 2002. A novel mutation (T65P) in the PAS domain of the human potassium channel HERG results in the long QT syndrome by trafficking deficiency. *J. Biol. Chem.* 277:48610–48616.

Priebe, L., and D. J. Beuckelmann. 1998. Simulation study of cellular electric properties in heart failure. *Circ. Res.* 82:1206–1223.

Sanguinetti, M. C., M. E. Curran, P. S. Spector, and M. T. Keating. 1996. Spectrum of HERG K^+-channel dysfunction in an inherited cardiac arrhythmia. *Proc. Natl. Acad. Sci. USA.* 93:2208–2212.

Sanguinetti, M. C., C. Jiang, M. E. Curran, and M. T. Keating. 1995. A mechanistic link between an inherited and an acquired cardiac arrhythmia: HERG encodes the I_{Kr} potassium channel. *Cell.* 81:299–307.

Sanguinetti, M. C., and N. K. Jurkiewicz. 1990. Two components of cardiac delayed rectifier K^+ current. Differential sensitivity to block by class III antiarrhythmic agents. *J. Gen. Physiol.* 96:195–215.

Seebohm, G., C. Lerche, A. E. Busch, and A. Bachmann. 2001. Dependence of I_{Ks} biophysical properties on the expression system. *Pflugers Arch.* 442:891–895.

Sharp, A. A., M. B. O'Neil, L. F. Abbott, and E. Marder. 1993. Dynamic clamp: computer-generated conductances in real neurons. *J. Neurophysiol.* 69:992–995.

Smith, P. L., T. Baukrowitz, and G. Yellen. 1996. The inward rectification mechanism of the HERG cardiac potassium channel. *Nature.* 379:833–836.

Snyders, D. J., and A. Chaudhary. 1996. High affinity open channel block by dofetilide of HERG expressed in a human cell line. *Mol. Pharmacol.* 49:949–955.

Sperelakis, N., and H. K. Shumaker. 1968. Phase-plane analysis of cardiac action potentials. *J. Electrocardiol.* 1:31–41.

Tan, R. C., and R. W. Joyner. 1990. Electrotonic influences on action potentials from isolated ventricular cells. *Circ. Res.* 67:1071–1081.

ten Tusscher, K. H., D. Noble, P. J. Noble, and A. V. Panfilov.2004. A model for human ventricular tissue. *Am. J. Physiol. Heart Circ. Physiol.* 286:H1573–H1589.

Trudeau, M. C., J. W. Warmke, B. Ganetzky, and G. A. Robertson. 1995. HERG, a human inward rectifier in the voltage-gated potassium channel family. *Science.* 269:92–95.

Verkerk, A. O., M. W. Veldkamp, A. C. van Ginneken, and L. N. Bouman. 1996. Biphasic response of action potential duration to metabolic inhibition in rabbit and human ventricular myocytes: role of transient outward current and ATP-regulated potassium current. *J. Mol. Cell. Cardiol.* 28:2443–2456.

Wang, J., M. C. Trudeau, A. M. Zappia, and G. A. Robertson. 1998. Regulation of deactivation by an amino terminal domain in human ether-a-go-go-related gene potassium channels. *J. Gen. Physiol.* 112:637–647.

Weerapura, M., S. Nattel, D. Chartier, R. Caballero, and T. E. Hebert. 2002. A comparison of currents carried by HERG, with and without coexpression of MiRP1, and the native rapid delayed rectifier current. Is MiRP1 the missing link? *J. Physiol.* 540:15–27.

Wilders, R., R. Kumar, R. W. Joyner, H. J. Jongsma, E. E. Verheijck, D. Golod, A. C. van Ginneken, and W. N. Goolsby. 1996. Action potential conduction between a ventricular cell model and an isolated ventricular cell. *Biophys. J.* 70:281–295.

Yamashita, T., Y. Murakawa, N. Hayami, E. Fukui, Y. Kasaoka, M. Inoue, and M. Omata. 2000. Short-term effects of rapid pacing on mRNA level of voltage-dependent K^+ channels in rat atrium: electrical remodeling in paroxysmal atrial tachycardia. *Circulation.* 101:2007–2014.

Zhou, Z., Q. Gong, B. Ye, Z. Fan, J. C. Makielski, G. A. Robertson, and C. T. January. 1998. Properties of HERG channels stably expressed in HEK 293 cells studied at physiological temperature. *Biophys. J.* 74:230–241.